Available online at www.sciencedirect.com

ScienceDirect

journal homepage: www.elsevier.com/locate/he

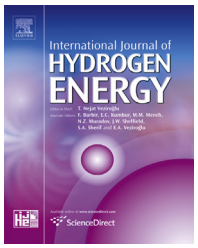

# Micro-contacted self-assembled tungsten oxide nanorods for hydrogen gas sensing

Stanislav Haviar [b,*], Šárka Chlupová [a], Peter Kúš [a], Marcel Gillet [a,1], Vladimír Matolín [a], Iva Matolínová [a]

[a] Department of Surface and Plasma Science, Faculty of Mathematics and Physics, Charles University, V Holešovičkách 2, 18000 Prague 8, Czech Republic

[b] Department of Physics and NTIS – European Centre of Excellence, University of West Bohemia, Univerzitní 8, 30614 Plzeň, Czech Republic

ARTICLE INFO

*Article history:*
Received 18 July 2016
Received in revised form
23 September 2016
Accepted 27 September 2016
Available online 21 November 2016

*Keywords:*
Gas sensor
Tungsten oxide
Hydrogen sensing
Nanorods
Nanofabrication
Electron beam lithography

ABSTRACT

Electron beam lithography was used to fabricate platinum $\mu$-contacts over tungsten oxide nanorods formed on a mica substrate. This made possible the measurement of sensorial response of these self-assembled tungsten oxide nanorods to hydrogen gas for the first time. The nanorods were prepared by thermal evaporation from an oxide source. Consequently, two types of conductometric sensors were assembled: a) percolating network of nanorods and b) set of individually contacted $WO_3$ nanorods. The preparation procedures are described in detail and the comparison of response of both types of assemblies is given. The first sensorial measurements revealed a good response of the b) type of sensor and the minimum repeatedly detected concentration of $H_2$ was 50 ppm.



## Introduction

In recent years, electrical sources based on hydrogen technologies have been attracting much attention as one of the most promising clean energy sources for the future. Devices using hydrogen as a fuel produce only water as a product and therefore do not require any monitoring for toxic pollutants in contrast to conventional combustion engines. However, there is a considerable demand for development of sensors that are able to monitor $H_2$ concentration on the ppm scale. Such highly sensitive sensors are a necessity not only for the safe handling and storage of the hydrogen fuel but they are also a key requirement for precise control of the hydrogen gas dosing for vulnerable energy sources such as fuel cells [1,2].

One of the promising materials capable of detection on the ppm scale is tungsten oxide. $WO_3$ was proved to be sensitive to a broad range of both oxidizing and reducing gases such as $NO_2$ [3,4], $O_3$ [5], $H_2S$ [4], $C_2H_6O$ [5,6] and $H_2$ [6–12]. Similarly, as in the case of other metal oxides used for gas sensor applications, there is a considerable effort to improve both the selectivity and sensitivity of tungsten oxide based sensors. This is preferably achieved by using various dopants (Pd, Pt, Au) [5,7–11,13] and/or by reducing the dimensions of the

* Corresponding author.
E-mail address: haviar@ntis.zcu.cz (S. Haviar).
[1] Deceased

http://dx.doi.org/10.1016/j.ijhydene.2016.09.187

sensitive material. Such reduction is done by utilizing thin layers prepared by various methods [14–18] or complexes formed by nano-objects such as nano-rods [3], wires [10,19], sheets [20] or clusters [21]. The formation of nano-sized tungsten oxide brings new properties to the material which leads to improvement of the gas sensing properties.

In this work we describe the utilization of a unique system of tungsten oxide nanorods. We were able to prepare platinum $\mu$-contacts by electron beam lithography (EBL). This enabled us to measure sensorial response to hydrogen for the first time. Moreover not only the conductivity of a percolating network of the nanorods was measured but also the response of a set of individually contacted nanorods could be recorded.

The nanorods were grown epitaxially on cleaved mica surface by thermal evaporation of $WO_3$ powder [22,23]. The initial phase of growth was affected by the potassium present on the cleaved surface of the mica. In the beginning, thin rods were formed by hexagonal tungsten bronze $K_xWO_3$ ($0.13 < x < 0.33$). After depleting potassium contained in mica, rods grow both in thickness and height, forming monoclinic $WO_3$. In Refs. [22,24], we reported high-resolution transmission electron microscopy (HR-TEM) and reflection high-energy electron diffraction (RHEED) studies that revealed this two-step growth of $WO_3$ rods. The detailed study in Ref. [25] including x-ray diffraction analyses (XRD) and SEM imaging also confirms the monoclinic structure of the prepared nanorods. Fig. 1 shows a sketch of the two types of nanorods with their typical dimensions.

It was proved in the references [26,27] that the rods are electrically conductive and therefore suitable for conductometric gas sensing experiments. Previously, this system was studied as a $NO_2$ sensor equipped with gold contacts prepared by optical lithography [3]. However the used assembly allowed measurement only of dense percolating network of nanorods.

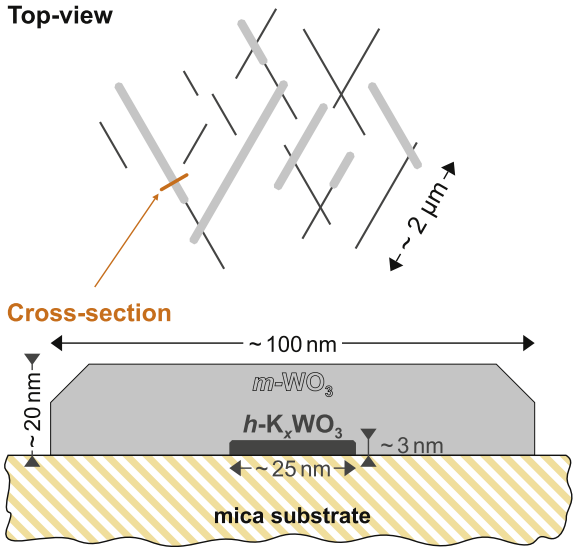


**Fig. 1 – Schematic drawing of the tungsten oxide nanorods grown by thermal evaporation on the muscovite mica surface. At first, tiny rods of hexagonal tungsten bronze ($K_xWO_3$, where $x < 0.3$) grow. Thereafter, wider and thicker rods formed by monoclinic $WO_3$ grow on top of some of the tiny rods. Typical dimensions are denoted in the drawing.**

The unique growth mechanism which occur only on mica allows the growth of nanorod network with various dimensions and also density. Moreover the instrumental setup is very simple and does not require time-consuming and expensive nanofabrication methods for preparing of nanorods.

Recently, we developed a simple method of preparation of metal (Au) nanowires on clean cleaved mica by electron beam lithography (EBL) [28]. Since the substrate is poorly conductive the EBL process had to be precisely optimized. Here, the electron beam lithography method was adapted for preparation of platinum $\mu$-wires aligned with prepared $WO_3$ rods. This allowed to contact individually a series of rods and thus to assemble a functional prototype of a conductometric hydrogen sensor. Using this arrangement we were able to measure the sensorial response of this unique system to hydrogen for the first time. The minimum detected concentration was 50 ppm.

## Experimental method

### *Sensing device preparation*

$WO_3$ nanorods were self-assembled on the surface of as-cleaved muscovite substrate during a vapor deposition process. The deposition was carried out using a planar source of $WO_3$ heated to 600 °C placed at a distance of 1 mm from the mica plate with dimensions of 10 × 14 $mm^2$ in the ambient atmosphere. The deposition time was 10 min and temperature of mica was measured to be around 400 °C. Further details of the experimental setup can be found in Ref. [23].

The morphology of the prepared nanorods was observed by a scanning electron microscope (SEM) Mira 3 (Tescan) in both backscattered (BSE) and secondary (SE) electron modes using electrons of primary energy of 30 keV.

The cleaved surface of mica suffers from inhomogeneity which leads to the existence of isolated areas with various densities of the $WO_3$ nanorods. Therefore it was necessary to make a reconnaissance of the sample surface and to identify suitable samples for further processing. On the basis of the SEM imaging, several samples were selected. The main criterion was the existence of a homogeneous coverage of the mica surface with the nanorods.

Furthermore, the mica substrates were equipped with two parallel platinum macro-contacts (electrodes) with an inner distance of 800 µm in order to measure the conductivity of the samples. The electrodes were sputter deposited through a shielding mask made of a steel sheet. The edges of the shielding mask did not fit the substrate absolutely tightly so the margins of the deposited contacts were not sharp-ended, and there was a gradient of material thickness observable in SEM. The width of not-covered area between the contacts varied from 400 to 700 µm. The sputtering process was carried out in the coating device MED 020 (Bal-Tec) using an unbalanced magnetron in dc mode with a metal Pt target (99.996% purity, 50 mm diameter). The target–substrate distance was 90 mm. Argon at a pressure of 0.8 Pa was used as a working gas, the discharge current was kept at 15 mA. The thickness of the deposited layer was controlled by a quartz thickness monitor; 70 nm of platinum was deposited at a rate of 3 nm/min.

Subsequently, the selected samples were processed by means of electron beam lithography (EBL) allowing us to precisely place the $\mu$-wires to overlap the $WO_3$ nanorods in order to ensure their electrical connection to the macro-contacts. A double-layer resist film was spin-coated onto the samples. Polymethylmethacrylate (PMMA) of two different molecular weights diluted in anisole was used as a resist material. The preparation parameters of the resist double layer can be found in Table 1.

The EBL exposition of the resist-coated sample was carried out using a dedicated DrawBeam software module directly in the SEM chamber at a working distance of 9 mm. An electron beam of 30 keV primary energy and current value of 200 pA was focused to a spot of 4 nm in diameter. The applied dose for creating the linear structures was 12 nC/cm. Since the SEM is digitally operated the lines were exposed as a series of points with 60 nm spacing and 360 μs dwell time. A scheme of geometrical arrangement of the exposed pattern is shown in Fig. 2. The development process was performed by rinsing the sample with isopropyl alcohol:water (3:7) solution for 40 s. The developed structures were consequently coated by 30 nm of Pt using the same setup as for the deposition of the electrodes. The process was completed by ultrasonically assisted lift-off in acetone with duration of 20 s. The schematic drawing of the sample preparation process flow is sketched in Fig. 3.

The samples were cautiously investigated by SEM after most of the process steps. This enabled us to pick proper samples for sensor measurements. Two types of samples were examined:

a) "Network" type samples were equipped only with macroscopic electrodes, see Fig. 3b. It was the case when the concentration of the rods was sufficiently high to form a percolating network with dimensions of the uniformly rod-covered areas large enough for deposition of the platinum macro-contacts. Therefore it was possible to perform the two-point conductivity measurements.
b) "Individual-rod" type samples were processed by EBL to equip the macroscopic electrodes by overlapping platinum $\mu$-wires, see Fig. 3f. Pitch and orientation of the Pt $\mu$-wires were adjusted individually for each sample with respect to length and orientation of the nanorods. This approach, suitable also for samples which do not form a percolating network of the rods, ensured the contact to both ends of averaged sized nanorods.

**Table 1 – Parameters of spin-coating (double layered PMMA on cleaved mica).**

| Spin-coating parameter | Bottom layer | Top layer |
|---|---|---|
| Thickness | 240 nm | 40 nm |
| $M_W$[a] | 120 K | 996 K |
| Solution conc.[b] | 5% wt. | 1% wt. |
| Speed | 2 krpm | 6 krpm |
| Duration | 60 s | |
| Acceleration duration | 8 s | |
| Soft-bake temp. | 195 °C | |

[a] Relative molecular weight.
[b] PMMA diluted in anisole.

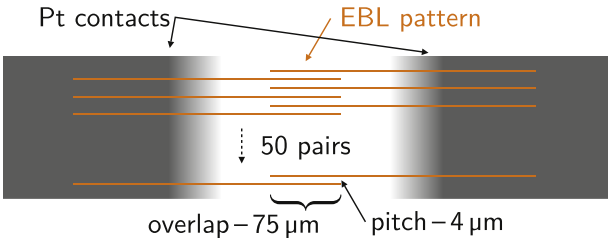


**Fig. 2 – Schematic drawing (multiple scaling) of exposed EBL pattern. There are 50 pairs of lines going opposite to each other from the pre-sputtered Pt contacts and overlapping in the central area.**

### *Measurement of gas sensing properties*

A self-designed station for sensor-testing was built to test conductometric sensors in a form of thin layers or nano-structured materials contacted by macroscopic electrodes. The sample was placed in a stainless steel chromium-coated chamber with volume of approximately 9 $cm^3$. The sensor was heated by a Boralectric® heating element (Tectra) encased with a thermocouple-monitored copper heating plate. The temperature can be controlled within the range from room temperature up to 400 °C. Three mass flow controllers (Alicat Scientific, various flow ranges) were used to regulate the portions of $N_2$, $O_2$ and $H_2$ gases in testing atmosphere which was introduced into the chamber in the continuous-flow regime. The exhaust of the system is open to the atmospheric pressure. In order to eliminate the thermal effects, the total flow was kept at a constant value of 120 sccm during all measurements, *i.e.*, for all concentrations and all working temperatures.

The electrical contact was realized by gold-plated spring-loaded tips which were pressed to the platinum contacts on the sample. The resistance measurements were conducted in the regime of constant voltage of 5 V and 1.2 V for the network and individual-rods types of the samples, respectively. Voltage and current were monitored by A/D converter (14 bit, 2 kS/s).

All samples were tested separately using a similar protocol. Prior to the measurement the samples were heated up to 300 °C and kept at this temperature for two hours. Constant flow of synthetic air was let into the chamber already during the heating. Afterwards, the sample was exposed to progressively changing concentrations of hydrogen with total gas flow unchanged. Each sample was tested at several working temperatures. Synthetic air was replaced by clean $N_2$ for reference measurements. The sensing response $S$ of the sensor to concentration $c$ of $H_2$ was evaluated by using the relation:

$$S = \frac{R_0 - R_c}{R_c}, \quad (1)$$

where $R_0$ is the resistance of the sample in synthetic air and $R_c$ is the resistance of the sample to concentration $c$ of $H_2$. The saturation values $R_0$ and $R_c$ were obtained by fitting the time dependencies of recovery process and response, respectively.

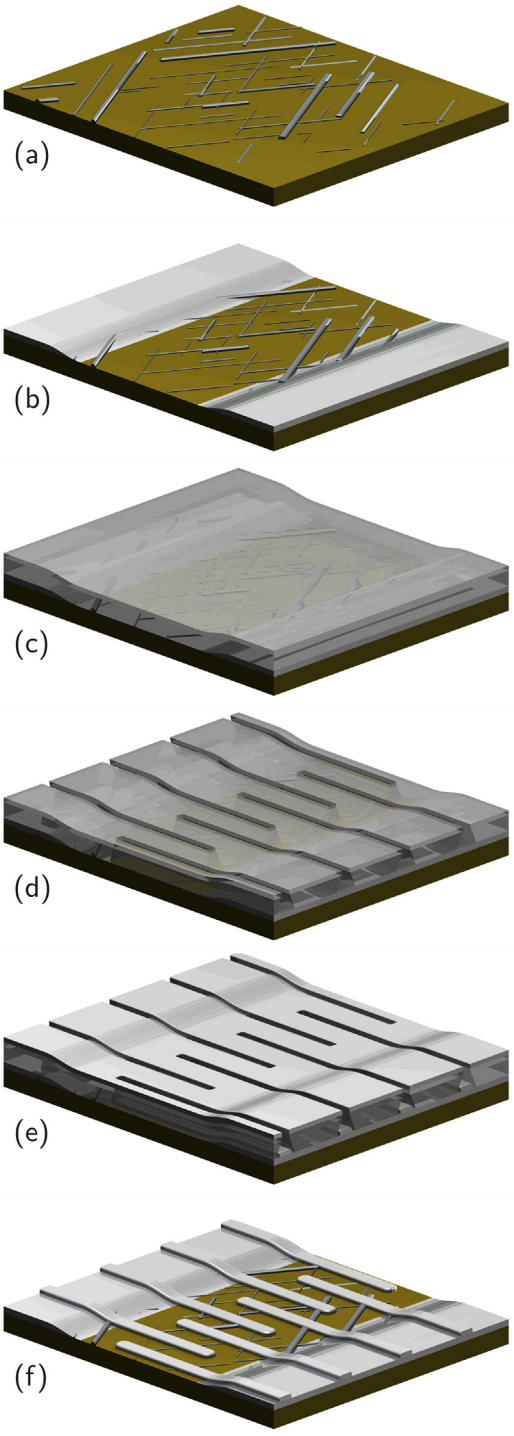


**Fig. 3 – Process flow of the sample preparation (of EBL pattern). (a) mica substrate with grown $WO_3$ nanorods, (b) sputter deposited Pt contacts, (c) spin-coated double-layer resist PMMA, (d) exposition and development, (e) Pt layer deposited, (f) resist stripped by ultrasonically assisted lift-off.**

## Results and discussion

### *EBL and SEM results*

Fig. 4 shows SEM micrographs of both types of the prepared sensors taken in the SE mode. The image contrast is given by charging effects on the mica substrate due to its poor conductivity contrary to tungsten oxide nanorods. Therefore bright pillow-shaped patterns are visible. Normally, this effect is undesirable for acquiring SEM micrographs, and other imaging modes must be used (*e.g.* BSE mode, low vacuum SEM) which often suffers from poorer resolution. In Fig. 5 there is a comparison of SE and BSE images of the individual-rod type sensor surface. Clearly the BSE image (Fig. 5b) cannot display all the rods visible in the SE mode due to the surface charge highlighting (Fig. 5a).

The micrographs shown in Figs. 3–5 demonstrate that the surface charge is led away by the nanorods connected to the Pt $\mu$-wires. This is a direct proof of conductive junctions between the wires and the tungsten oxide nanorods. The nanorods which do not touch the grounded Pt $\mu$-wires are clouded over with the surface charge as it can be seen in the area labeled "A" of Fig. 6. Moreover, rods in the area labeled "B" demonstrate the fact that the mutual junctions between two nanorods are conductive, too. This is in good correspondence with conductivity atomic force microscopy measurements presented in Ref. [27].

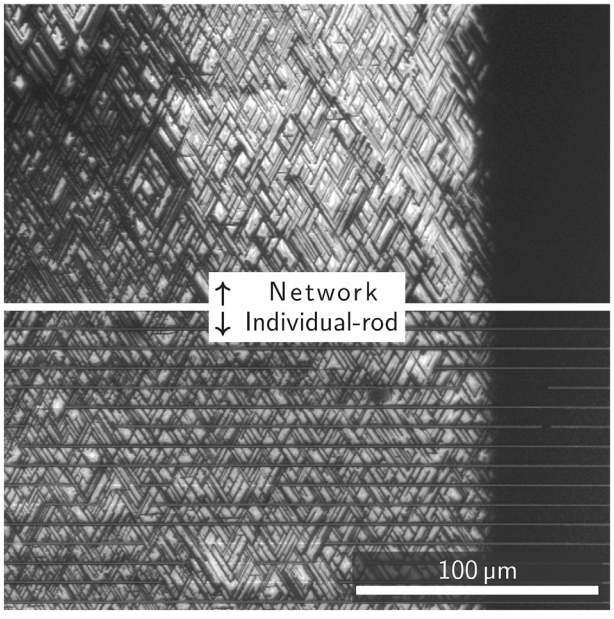


**Fig. 4 – SEM (SE mode) micrograph of the prepared sensor. The edge of the Pt macro contact is visible on the right hand side. The top half of the image represents the typical appearance of a network type of sample with percolating dense network of nanorods. The bottom part of the image shows Pt $\mu$-wires crossing an individual-rod type of sample, where most of rods are connected directly to the metal $\mu$-wires. The bright texture appears due to the charging effects (discussed in text).**

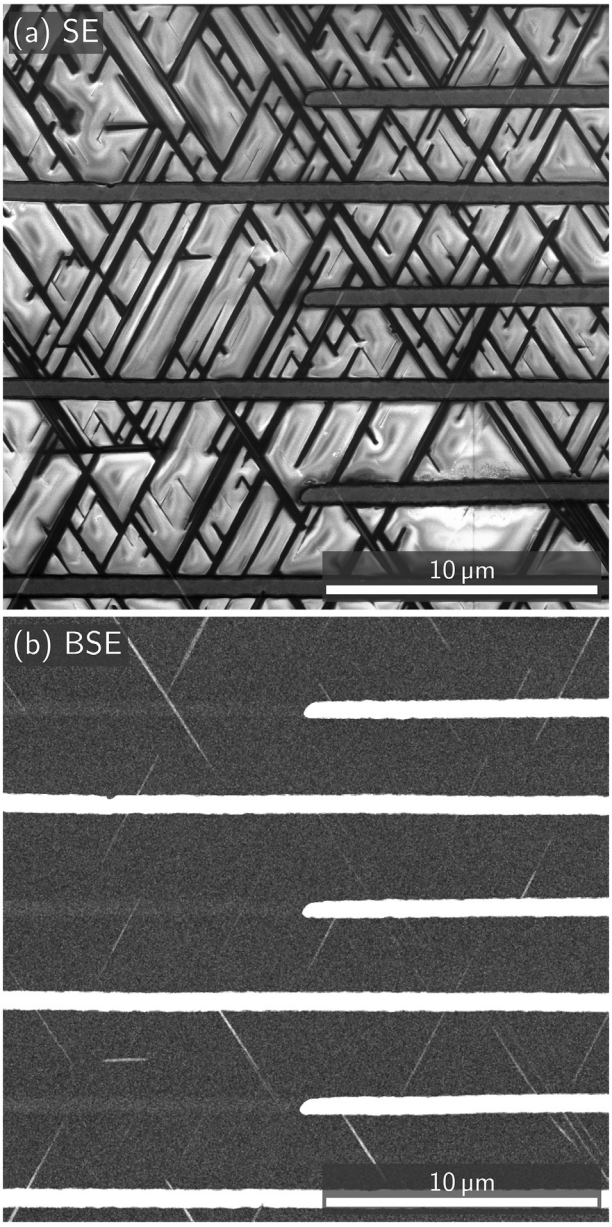


**Fig. 5 – SEM micrographs of the same area in the middle of the lithographically prepared sensor taken in different view modes. Surface charging effect observable in secondary electron mode (a) highlights the rods which are indistinguishable in the view of backscattered electrons (b).**

For each tested sample SEM overviews were imaged in order to estimate the active sensing area. The network-type sample analyzed had the inner distance between contacts of approximately 400 μm. The length of the contacts was 12 mm; however the percolating network of the nanorods was present only between segments which have approximately 2 mm in length in a sum. Therefore we can estimate the active area to be (1.0 ± 0.2) $mm^2$. The density of rods observable by SEM in the SE mode varied considerably over the covered area. Therefore, the total number of rods connected to the network can be estimated only roughly. If we assume density (0.02 ± 0.01) rods per $\mu m^2$ the overall number of rods was on

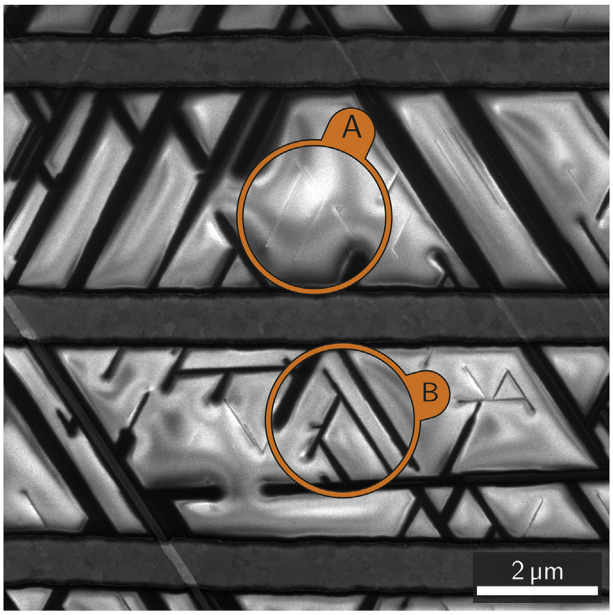


**Fig. 6 – SEM micrographs of the Pt μ-wires contacting the $WO_3$ nanorods. In the area labeled A there are rods which are not in contact with any grounded object and therefore they are flooded by the surface charge appearing as white pattern in SE. The rods present in the area B are connected to other rods grounded by Pt wire and the charge is "sucked out" from their surroundings.**

the order of tens of thousands. There were hundreds of rods in direct contact to the platinum electrodes.

Fig. 7 shows an overview of a tested individual-rod sensor prototype. The manufacturing defects in the form of interrupted Pt wires, which are visible in the micrograph, were caused by the irregularities of the mica substrate. The simple

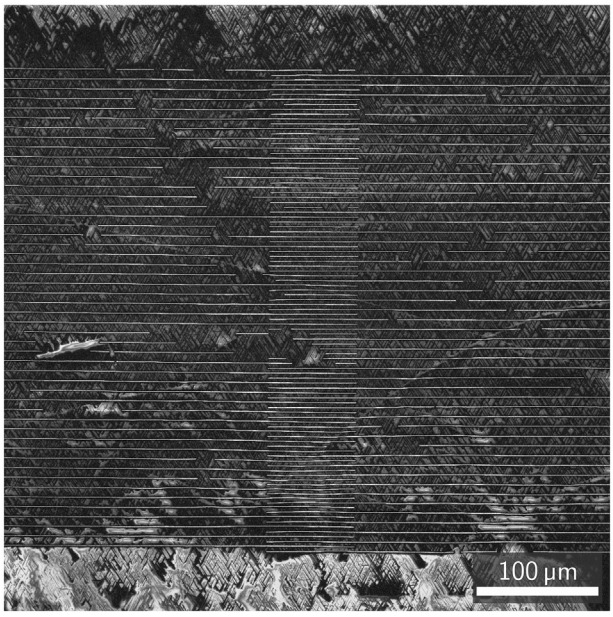


**Fig. 7 – SEM micrograph of prepared sensor with Pt μ-contacts. The SE and BSE signals were combined for better distinctiveness of all features.**

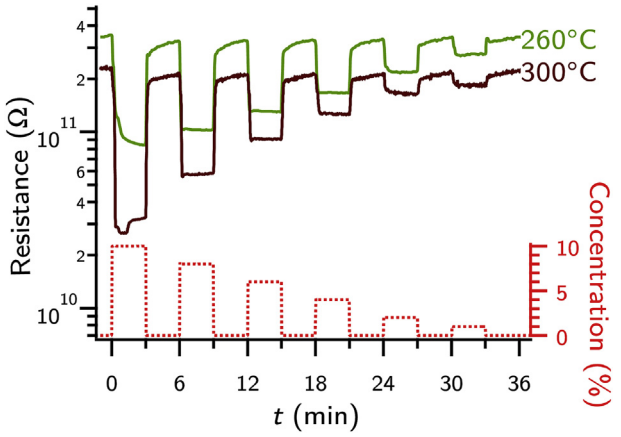


**Fig. 8 – Response of the network type sample to changing concentrations of $H_2$ carried in the synthetic air at different temperatures.**

EBL process with the basic double-layer resist did not guarantee the complete reliability. Nevertheless, it was possible to count the pairs of uninterrupted wires; for this sample there were 21 complete pairs. The width of the Pt $\mu$-wire was measured to be (0.77 ± 0.02) μm. The dimensions presented in Fig. 2, i.e., the length of the $\mu$-wires overlap and their mutual distance, allowed us to estimate the contacted sensing area to be 5000 $\mu m^2$. The density of rods directly connected to 100 μm of μ-wire was counted to be 60 ± 9. This gives the total number of rods contacted by two nearest wires to be approximately 1000. Since almost all of the nanorods enclose the same angle with the $\mu$-wires, average active length of each rod was calculated to be 4 μm.

### *Gas sensing properties*

The sensing response of the network type sample for two working temperatures of 260 °C and 300 °C is depicted in Fig. 8, where $H_2$ concentrations range from 10% down to 1%. The minimum detectable concentration for this type of samples was 0.1%. The values of sensing response are discussed below. The saturation value for synthetic air without hydrogen was stable, and response and recovery times are comparable for this range of concentrations, see Table 2.

Fig. 9a shows the sensor response of the individual-rod sample to gradually increasing concentration of $H_2$ from 0.1% to 1% for three working temperatures of 150, 300 and 410 °C. The largest relative response was observed for the lowest used working temperature. However, due to the lengthy response time for low temperatures, the responses to concentrations lower than 1000 ppm were acquired at 300 °C. At this temperature the samples were stable enough to obtain a reproducible response. The minimum tested concentration of $H_2$ in synthetic air was 50 ppm. The relative response versus time dependency to concentrations from 50 to 1000 ppm of hydrogen is plotted in Fig. 9b. Note that the measurements presented in Fig. 9a and b were acquired on two samples which differ in the density of the tungsten oxide nanorods. The higher the nanorod density is, the lower the electrical resistance, since the nanorods can be considered as resistors connected in parallel configuration. The lower resistance values presented in Fig. 9b correspond to the sample depicted in Figs. 4–6.

Both the response and recovery time dependencies can be fitted by a sum of two exponential functions:

$$R(t) = R_{0,c} + A_1 \cdot e^{-t/\tau_1} + A_2 \cdot e^{-t/\tau_2}, \quad (2)$$

because the commonly used single exponential function does not provide accurate fit. The values $R_c$ and $R_0$ denotes the saturation values of resistivity R ($A_{1,2}$ and $\tau_{1,2}$ are amplitudes and time constants of the exponential fit). The fitted parameters for the resistance dependence on time evaluated for both the types of samples at 300 °C for 1% concentration of $H_2$ can be found in Table 2. The coefficient of determination ($R^2$) reaches values above 0.99 for all measurements of the individual-rod type samples. For the network type sample, the double exponential function fits well for higher concentrations. For the concentration of 1%, the $R^2$ is considerably

**Table 2 – Comparison of the response and recovery kinetics for both types of samples.**

| | Individual-rod type | | Network type | | |
|---|---|---|---|---|---|
| | Response | Decay | Response | Decay | |
| $R_S$ | $27 \times 10^6$ | $77 \times 10^6$ | $170 \times 10^9$ | $200 \times 10^9$ | Ω |
| $A_1$ | $40 \times 10^6$ | $-32 \times 10^6$ | $17 \times 10^9$ | $-6.8 \times 10^9$ | Ω |
| $\tau_1$ | 4 | 6 | 15 | 5 | s |
| $A_2$ | $80 \times 10^5$ | $-20 \times 10^6$ | $10 \times 10^9$ | $-24 \times 10^9$ | Ω |
| $\tau_2$ | 30 | 120 | 45 | 110 | S |
| $R^2$ | 0.998 | 0.999 | 0.824 | 0.715 | |
| $\tau_{90\%}$ | 18 | 170 | 60 | 220 | s |
| S | 1.8 | | 0.17 | | |

The time ($t$) versus resistance ($R$) characteristics were fitted with a function $R(t) = R_{0,c} + A_1 \cdot e^{-t/\tau_1} + A_2 \cdot e^{-t/\tau_2}$.

$R_S$ – saturation value of resistance, $R^2$ – coefficient of determination, $\tau_{90\%}$ – period of reaching of 90% of difference between saturation values, $S$ – sensing response

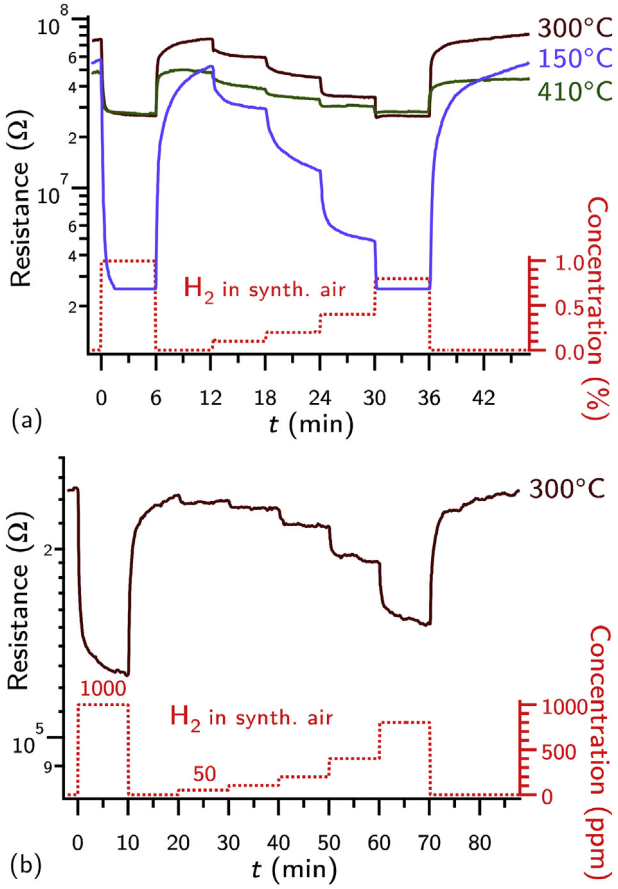


**Fig. 9 – Response of the EBL-processed (the individual-rod type) sample to various concentrations of $H_2$ carried in the synthetic air at different temperatures. (The response at 150 °C for the 1% of $H_2$ is not recorded completely due to the instrumental limitation.) In (b) there is the minimum detected concentration (50 ppm) presented at temperature of 300 °C.**

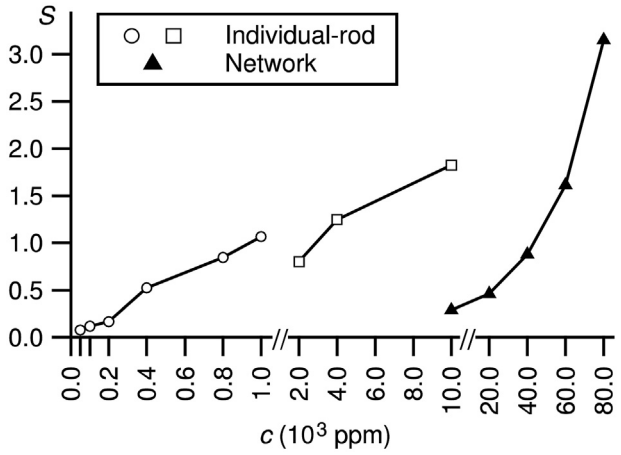


**Fig. 10 – Relative response S for various concentrations c (semi-logarithmic scale) of $H_2$ for two samples of the individual-rod type and one of the network type measured at the same temperature of 300 °C. The response of the network type sample reaches the similar values for $H_2$ concentrations of two orders higher.**

smaller mainly due to the high noise to signal ratio of the acquired data since the recorded current was only on the order of tens of pA.

The sensing response S as a function of $H_2$ concentration at 300 °C is plotted in Fig. 10. As expected, the value of the response increases with the hydrogen concentration. The drop of the S value around the concentration value of 1000 ppm for two different samples does not carry high importance since the data were measured on two samples of the individual-rod type at different voltages. The graph points out the key result that for samples with similar density of nanorods the arrangement of electrical contacts, consisting of the macro-electrodes coupled with EBL assisted μ-wires overlapping individual tungsten oxide nanorods, enhanced the sensitivity of the self-assembled tungsten oxide nanorods for hydrogen by a factor of ten (in case of 1000 ppm of $H_2$ at the working temperature of 300 °C).

Because of the uniqueness of the system, self-assembled $WO_3$ nanorods on the mica surface, the comparison to similar systems is difficult and/or speculative. The system was previously tested for response only to oxidizing gases [3]. The response of nanorod system to $NO_2$ was evaluated in a similar way: the response characteristics were described by conductivity vs. time measurements and these characteristics were fitted as a sum of two exponential function of time. The sensing mechanism is not discussed in this work. The description by two exponential functions with different relaxation times may confirm the two-process model of the $H_2$ sensing mechanism as described in Ref. [10]. In the study [10] the $WO_3$ nanowires were prepared by thermal evaporation with additional oxidation and doped by platinum nanoclusters all over their surface showed lower sensitivity and much longer response times.

The Pt doped $WO_3$ systems exhibit significantly better hydrogen-gas sensing properties than the undoped ones [11,16,29,30]. This is because of the rapid dissociation of adsorbed hydrogen on the Pt catalyst. Dissociated hydrogen species spill over onto the oxide and easily react [10,29,31–33]. This effect can also explain the enhanced sensitivity of the individual-rod type of sample in comparison to the network type. Also the higher sensitivity at lower temperatures (150 °C) indicates the influence of the catalyst (See Fig. 9a.). The contact of Pt with the tungsten oxide is localized only to the junctions of the rods and the μ-wires. If we, however, assume that the rods are formed by only a few grains [22,25,34], the reaction of hydrogen with the end parts of the μ-contacted rods plays a nonnegligible role in changing the overall conductivity of the nanorod. This is because the affected grain, which is in contact with the catalyst, is a considerable portion of the rod.

The role of Pt used as a contacting material was not quantified precisely since the attempts to use another metal (Au, Cr) for μ-contacts on the mica substrate did not meet the requirements for stable electrical measurements. But generally, it can be assumed that adding Pt also in between the μ-contacts would improve the sensor response even more.

## Conclusions

In summary, the samples with epitaxially grown tungsten oxide nanorods on muscovite-type mica were assembled into a form of a conductometric gas sensor. Nonpercolating $WO_3$ nanorods' conductivity measurement was made possible by their coating with accurately aligned, individual, platinum $\mu$-wires. The electrodes were prepared by means of electron beam lithography and SEM observations proved the conductive contact between the rods and wires.

The response of the percolating network of $WO_3$ nanorods was compared with the response of samples equipped with $\mu$-wires which contacted the nanorods separately. The assembly employing $\mu$-wires increased the sensitivity of the sensor by factor of 10 and lowered the minimum detectable concentration of hydrogen from 1000 ppm down to 50 ppm.

The measurements of the response to $H_2$ on this specific system were conducted for the first time and provided results which are comparable with other sensors based on tungsten oxide nanorods. However more detailed sensorial measurements, including also measurements of the stability of the sensor, are necessary for further evaluation of the sensorial potential of self-assembled tungsten oxide nanorods.

## Acknowledgments

The authors acknowledge financial support by the project LD13054 financed by the Czech Ministry of Education. P.K. appreciates support from Charles University in Prague, project GA UK No. 236214. S.H. would like to thank the European Regional Development Fund under Project "NTIS – New Technologies for Information Society", European Centre of Excellence, CZ.1.05/1.1.00/02.0090.

## REFERENCES

[1] Hübert T, Boon-Brett L, Black G, Banach U. Hydrogen sensors – a review. Sensors Actuators B Chem 2011;157:329–52. http://dx.doi.org/10.1016/j.snb.2011.04.070.

[2] Boon-Brett L, Bousek J, Black G, Moretto P, Castello P, Hübert T, et al. Identifying performance gaps in hydrogen safety sensor technology for automotive and stationary applications. Int J Hydrogen Energy 2010;35:373–84. http://dx.doi.org/10.1016/j.ijhydene.2009.10.064.

[3] El Achhab M, Shanak H, Schierbaum K. $NO_2$ sensing properties of $WO_3$ nanorods grown on mica. Phys Status Solidi 2011;208:1229–34. http://dx.doi.org/10.1002/pssa.201000960.

[4] Hoel A, Reyes LF, Heszler P, Lantto V, Granqvist CG. Nanomaterials for environmental applications: novel $WO_3$-based gas sensors made by advanced gas deposition. Curr Appl Phys 2004;4:547–53. http://dx.doi.org/10.1016/j.cap.2004.01.016.

[5] Labidi A, Gillet E, Delamare R, Maaref M, Aguir K. Ethanol and ozone sensing characteristics of $WO_3$ based sensors activated by Au and Pd. Sensors Actuators B Chem 2006;120:338–45. http://dx.doi.org/10.1016/j.snb.2006.02.015.

[6] Yu-De W, Zhan-Xian C, Yan-Feng L, Zhen-Lai Z, Xing-Hui W. Electrical and gas-sensing properties of $WO_3$ semiconductor material. Solid State Electron 2001;45:639–44. http://dx.doi.org/10.1016/S0038-1101(01)00126-5.

[7] Zhang C, Boudiba A, Navio C, Bittencourt C, Olivier M-G, Snyders R, et al. Highly sensitive hydrogen sensors based on co-sputtered platinum-activated tungsten oxide films. Int J Hydrogen Energy 2011;36:1107–14. http://dx.doi.org/10.1016/j.ijhydene.2010.10.011.

[8] Boudiba A, Roussel P, Zhang C, Olivier M-G, Snyders R, Debliquy M. Sensing mechanism of hydrogen sensors based on palladium-loaded tungsten oxide (Pd–$WO_3$). Sensors Actuators B Chem 2013;187:84–93. http://dx.doi.org/10.1016/j.snb.2012.09.063.

[9] Kim N, Seo CW, Cheong H. Improved durability of Pd/$WO_3$ hydrogen sensor films prepared by sputtering. J Korean Phys Soc 2008;52:50. http://dx.doi.org/10.3938/jkps.52.50.

[10] Zhu LF, She JC, Luo JY, Deng SZ, Chen J, Xu NS. Study of physical and chemical processes of $H_2$ sensing of Pt-Coated $WO_3$ nanowire films. J Phys Chem C 2010;114:15504–9. http://dx.doi.org/10.1021/jp106460w.

[11] Zhang C, Kanta AF, Yin H, Boudiba A, D'Haen J, Olivier MG, et al. $H_2$ sensors based on $WO_3$ thin films activated by platinum nanoparticles synthesized by electroless process. Int J Hydrogen Energy 2013;38:2929–35. http://dx.doi.org/10.1016/j.ijhydene.2012.12.017.

[12] Ou JZ, Campbell JL, Yao D, Wlodarski W, Kalantar-Zadeh K. In situ Raman spectroscopy of H2 gas interaction with layered $MoO_3$. J Phys Chem C 2011;115:10757–63. http://dx.doi.org/10.1021/jp202123a.

[13] Esfandiar A, Irajizad A, Akhavan O, Ghasemi S, Gholami MR. Pd-$WO_3$/reduced graphene oxide hierarchical nanostructures as efficient hydrogen gas sensors. Int J Hydrogen Energy 2014;39:8169–79. http://dx.doi.org/10.1016/j.ijhydene.2014.03.117.

[14] Penza M, Martucci C, Cassano G. NOx gas sensing characteristics of $WO_3$ thin films activated by noble metals (Pd, Pt, Au) layers. Sensors Actuators B Chem 1998;50:52–9. http://dx.doi.org/10.1016/S0925-4005(98)00156-7.

[15] Stankova N, Calderer J, Vilanova X, Llobet E, Gracia I, Cane C, et al. Improvement of the gas sensing properties of rf sputtered $WO_3$ thin films using different dopants. Conf. Electron Devices, 2005 Spanish, IEEE; 2005, p. 553–6. http://dx.doi.org/10.1109/SCED.2005.1504512.

[16] Yamaguchi Y, Emoto Y, Kineri T, Fujimoto M, Mae H, Yasumori A, et al. Hydrogen gas-sensing properties of Pt/$WO_3$ thin film in various measurement conditions. Ionics (Kiel) 2012;18:449–53. http://dx.doi.org/10.1007/s11581-012-0683-2.

[17] Di Giulio M, Manno D, Micocci G, Serra A, Tepore A. Sputter deposition of tungsten trioxide for gas sensing applications. J Mater Sci Mater Electron 1998;9:317–22. http://dx.doi.org/10.1023/A:1008889009741.

[18] Zhao M, Huang J, Ong C-W. Feasibility of H2 sensors composed of tungsten oxide nanocluster films. Int J Hydrogen Energy 2013;38:15559–66. http://dx.doi.org/10.1016/j.ijhydene.2013.09.069.

[19] Choi KJ, Jang HW. One-dimensional oxide nanostructures as gas-sensing materials: review and issues. Sensors 2010;10:4083–99. http://dx.doi.org/10.3390/s100404083.

[20] Kalantar-Zadeh K, Vijayaraghavan A, Ham MH, Zheng H, Breedon M, Strano MS. Synthesis of atomically thin $WO_3$ sheets from hydrated tungsten trioxide. Chem Mater 2010;22:5660–6. http://dx.doi.org/10.1021/cm1019603.

[21] Szabó M, Pusztai P, Leino A-R, Kordás K, Kónya Z, Kukovecz Á. Synthesis and characterization of $WO_3$ nanowires and metal nanoparticle-$WO_3$ nanowire composites. J Mol Struct 2013;1044:99–103. http://dx.doi.org/10.1016/j.molstruc.2012.11.041.

[22] Mašek K, Gillet M, Matolín V. Evidence for two growth modes during tungsten oxide vapor deposition on mica substrates. J

Cryst Growth 2014;394:67–73. http://dx.doi.org/10.1016/j.jcrysgro.2014.02.026.
[23] Gillet M, Delamare R, Gillet E. Growth of epitaxial tungsten oxide nanorods. J Cryst Growth 2005;279:93–9. http://dx.doi.org/10.1016/j.jcrysgro.2005.01.089.
[24] Gillet M, Masek K, Potin V, Bruyère S, Domenichini B, Bourgeois S, et al. An epitaxial hexagonal tungsten bronze as precursor for $WO_3$ nanorods on mica. J Cryst Growth 2008;310:3318–24. http://dx.doi.org/10.1016/j.jcrysgro.2008.03.040.
[25] Matolínová I, Gillet M, Gillet E, Matolín V. A study of tungsten oxide nanowires self-organized on mica support. Nanotechnology 2009;20:445604. http://dx.doi.org/10.1088/0957-4484/20/44/445604.
[26] Gillet M, Delamare R, Gillet E. Structure and electrical conduction of $WO_3$ nanorods epitaxially grown on mica. Eur Phys J D 2007;43:295–8. http://dx.doi.org/10.1140/epjd/e2007-00101-2.
[27] Gillet M, Delamare R, Gillet E. Growth, structure and electrical conduction of $WO_3$ nanorods. Appl Surf Sci 2007;254:270–3. http://dx.doi.org/10.1016/j.apsusc.2007.07.124.
[28] Haviar S, Gillet M, Matolínová I. E-beam lithography processing of Au-nanowire contacts for development of gas sensors based on tungsten-oxide nanorods self-assembled on mica. Int J Nanotechnol 2012;9:825, http://dx.doi.org/10.1504/IJNT.2012.046755.
[29] Zhang J, Liu X, Xu M, Guo X, Wu S, Zhang S, et al. Pt clusters supported on $WO_3$ for ethanol detection. Sensors Actuators B Chem 2010;147:185–90. http://dx.doi.org/10.1016/j.snb.2010.03.017.
[30] Samerjai T, Liewhiran C, Wisitsoraat A, Tuantranont A, Khanta C, Phanichphant S. Highly selective hydrogen sensing of Pt-loaded $WO_3$ synthesized by hydrothermal/impregnation methods. Int J Hydrogen Energy 2014;39:6120–8. http://dx.doi.org/10.1016/j.ijhydene.2014.01.184.
[31] Yaacob MH, Breedon M, Kalantar-zadeh K, Wlodarski W. Absorption spectral response of nanotextured $WO_3$ thin films with Pt catalyst towards $H_2$. Sensors Actuators B Chem 2009;137:115–20. http://dx.doi.org/10.1016/j.snb.2008.12.035.
[32] Ippolito SJ, Kandasamy S, Kalantar-Zadeh K, Wlodarski W. Layered SAW hydrogen sensor with modified tungsten trioxide selective layer. Sensors Actuators B Chem 2005;108:553–7. http://dx.doi.org/10.1016/j.snb.2004.11.048.
[33] Zheng H, Ou JZ, Strano MS, Kaner RB, Mitchell A, Kalantar-zadeh K. Nanostructured tungsten oxide - properties, synthesis, and applications. Adv Funct Mater 2011;21:2175–96. http://dx.doi.org/10.1002/adfm.201002477.
[34] Delamare R, Gillet M, Gillet E, Guaino P. Structure and electrical properties of tungsten oxide nanorods epitaxially organized on a mica substrate. Surf Sci 2007;601:2675–9. http://dx.doi.org/10.1016/j.susc.2006.12.081.